Radiolytic Corrosion of Uranium Dioxide: Role of Molecular Species

A. Traboulsi, Johan Vandenborre, G. Blain, Bernard Humbert, J. Barbet, M. Fattahi

Radiolytic Corrosion of Uranium Dioxide: Role of Molecular Species

Ali Traboulsi[1], *Johan Vandenborre*[*1], *Guillaume Blain*[1], *Bernard Humbert*[2], *Jacques Barbet*[3], *Massoud Fattahi*[1]

[1]SUBATECH, UMR 6457, Ecole des Mines de Nantes – CNRS/IN2P3, 4 rue Alfred Kastler, La Chantrerie BP 20722, 44307 Nantes cedex 3, France

[2]Institut des Matériaux Jean Rouxel, UMR 6502, Université de Nantes – CNRS, 2 rue de la Houssinière, BP 322229, 44340 Nantes, France

[3]Cyclotron Arronax, 1 rue Arronax, CS 10112, 44817 Saint Herblain cedex, France

Abstract

In this work, oxidative corrosion of UO_2 particles by molecular species produced by $^4He^{2+}$ radiolysis of water (simulated by irradiation with $^4He^{2+}$ beam) has been investigated as a function of the absorbed dose under open and closed atmosphere. This work was carried out by coupling for the first time: 1) characterization of the UO_2 surface after oxidation, 2) analysis of H_2 and H_2O_2 produced by water radiolysis and 3) quantification of the uranium species leached into the solution during irradiation. Oxidation of the surface of the UO_2 particles was characterized by Raman spectroscopy. H_2 and H_2O_2 were analyzed by micro gas chromatography and UV-VIS spectrophotometry respectively. Inductively coupled plasma mass spectrometry was used to quantify the soluble uranium species released into the solution. The results showed that when the ultra-pure water above the UO_2 particles was irradiated in open atmosphere, metastudtite was formed on the UO_2 surface indicating its oxidation by the H_2O_2 produced by water radiolysis. This oxidation was accompanied by migration of soluble uranium species (U(VI)) into the irradiated solution. After irradiation in closed atmosphere, oxidation of the UO_2 surface and migration of soluble uranium species were limited due to the presence of H_2. The inhibition does not occur by direct effect of H_2 on H_2O_2 but more probably by adsorption of H_2 molecules on the UO_2 surface.

Keywords: Water Radiolysis, UO_2 Radiolytic Corrosion, Raman Spectroscopy, Soluble Uranium, Chemical Yields.

1. Introduction

Management of nuclear waste as the spent nuclear fuel is one of the major political, social and scientific concerns in the countries using nuclear industry[1]. Among various management possibilities, the concept of direct disposal of this high level waste in deep geological vaults (500 to 1000 m of depth) is being seriously considered by several countries[2]. In this case, the spent nuclear fuel will be stored within canisters (from steel or copper) and its disposal is planned to be made in presence of a series of natural and artificial barriers whose aim is to protect the biosphere from an eventual radioactive contamination by insulating the waste from the outside environment[3]. However the impact of these disposal repositories on the environment over tens or hundreds of thousands of years is still being studied.

In the concept of deep geological disposal, groundwater is assumed to success within geological timescales ($\geq$ 300-1000 years)[4, 5] to percolate the different barriers and arrive to the nuclear waste package. Considering the scenario of canister failure, groundwater could get then in direct contact with the spent fuel. It is then crucial to study the behavior of the spent fuel in presence of water in real conditions encountered in deep geological sites in order to predict its possible dissolution mechanism, dissolution rate and thus, migration of radioactive elements to the environment. In fact, the spent nuclear fuel matrix is formed mainly by uranium dioxide (UO_2) with a small fraction (< 5%) of long-lived highly radiotoxic actinides and other fission products[1]. The majority of these radionuclides is trapped in the UO_2 matrix and the only credible mechanism of their migration into the environment is dissolution and transport by water in contact with the spent fuel. In this case, the releasing rate of these radionuclides is governed by the dissolution rate of the UO_2 matrix[6].

Groundwater present at the expected depth of deep geological repositories is generally reducing and spent fuel matrix (in its reduced form U(IV)) has a very low solubility in these conditions[2]. However, the reducing environment near the fuel surface may be altered by water

radiolysis caused by the radiation field associated to the spent fuel. Water radiolysis generates indeed various oxidants (e.g. O_2, H_2O_2, $OH^{\bullet}$…) [7-8] near the waste surface (about 30 - 40 µm) [9,2]. This leads to the oxidation of UO_2 to U(VI), a species more soluble than its reduced form (U(IV))[10] which favors the spent fuel dissolution and consequently the migration of radiotoxic elements from the repository to the biosphere[3]. On the other hand, it is known that the corrosion process is limited in presence of H_2 produced by water radiolysis due to its reducing properties [11-12]. Then, the knowledge of the chemistry of the solid-liquid interface (oxidation, corrosion…) which controls the radionuclide release under the conditions encountered in deep geological repositories is of great importance to ensure secure and safe management of this type of nuclear waste. However, it is not expected that groundwater reaches the spent fuel surface before few thousands of years of storage time[13]. At these geological timescales, short-lived radionuclides emitting principally β and γ rays will have been disappeared due to their radioactivity decay and the radiation field of the spent fuel will be mainly limited to α irradiation[2, 4].

In this work, we propose to investigate the effect of molecular species produced by $^4He^{2+}$ radiolysis of water on the UO_2 corrosion under controlled irradiation and environmental conditions.

Earlier papers relate that among all the products generated by water radiolysis, H_2O_2 is considered an important[14-16] and even the major [17, 18-19] actor in the oxidative dissolution of UO_2 under irradiation. The effect of O_2 on this latter process is considered negligible[20]. Moreover, some authors [17, 18-19] considered H_2O_2 as the unique oxidant to retain in UO_2 oxidation and dissolution, whereas others[14, 15] defend the idea that the effect of H_2O_2 is combined to that of radical radiolytic species. In presence of oxidant and in absence of complexing agent in the solution, oxidation of UO_2 starts by the formation of an oxidized phase on its surface[21, 22]. Characterization of the oxidized phase by XRD (X Ray Diffraction),

Raman Spectroscopy and XPS (X-ray Photoelectron Spectroscopy) showed that this phase is mainly formed of studtite (or metastudtite when dehydrated) corresponding to UO_4 in case of oxidation by H_2O_2 produced or not by water radiolysis[13, 14, 23]. Later, the oxidized phase undergoes a dissolution reaction in the form of U(VI) which may precipitate at sufficiently high oxidant concentrations on the UO_2 surface as secondary phase of schoepite (UO_3 xH_2O)[21, 22]. In deep geological repositories, this dissolution step leads to the migration of different radionuclides contained in the UO_2 matrix with a leaching rate depending on the UO_2 dissolution rate. Dissolution rate of UO_2 was investigated in the literature by quantifying the oxidized uranium species leached into water based on leaching and electrochemical experiments coupled sometimes to model calculations[6, 24-26]. The UO_2 dissolution rate varies widely with the irradiation conditions (irradiation source, irradiation environment, absorbed dose, dose rate…) which make it very difficult to compare the values obtained from different works.

The inhibitory effect of H_2 on the UO_2 corrosion process was largely investigated in the literature [11-12, 1]. In general, presence of H_2 during irradiation leads to diminution and even total inhibition of UO_2 dissolution. To explain this inhibition process, some authors[27] proposed a reduction mechanism based on radical interactions with the oxidized U(VI) released into solution.

Despite the high number of publications about UO_2 corrosion by the radiolytic products of water irradiated by $^4He^{2+}$ radiation, a distinction between the effect of radicals and molecular oxydants on this process was never realized. To the best of our knowledge, combination of solid corrosion characterization, analysis of H_2 and H_2O_2 produced by water radiolysis and quantification of soluble uranium species leached in to the solution during the oxidative dissolution of UO_2 was not reported in the literature. Also, the effect of H_2 produced by water

radiolysis has not been sufficiently investigated to have a complete understanding of the involved complicated inhibition mechanism.

The aim of this work was to investigate experimentally the effect of molecular radiolytic species (in particular H_2 and H_2O_2) produced by localized $^4He^{2+}$ radiolysis of water on UO_2 corrosion under different parameters encountered in deep geological repositories. Water in contact with the UO_2 particles was then irradiated by $^4He^{2+}$ beam at different absorbed doses under open and closed atmospheres in order to evaluate the effect of H_2 on the corrosion process. To fulfill this work, we chose to characterize the surface oxidation of the solid particles by Raman Spectroscopy which is known to be very efficient in surface characterization of solid state materials. It was used in some earlier works to investigate UO_2 corrosion under irradiation[28, 29]. Soluble uranium species leached into the solution were analyzed by Inducted Coupled Plasma Mass Spectrometry (ICP-MS) technique. H_2O_2 and H_2 produced by water radiolysis were quantified by UV-VIS Spectrophotometry and Gas Chromatography (μ-GC) respectively in order to calculate their radiolytic yields, compare them to those of pure water and clarify the role of these two species in the UO_2 corrosion process.

2. Materials and Methods

2.1. System studied: UO_2 Particles and Ultra pure Water

The material studied in this work is UO_2 TRistuctural-ISOtropic (TRISO) particles which were provided by Professor Fachinger of FZ-Jülich (Forschungszentrum Jülich) and their synthesis is detailed in the work of Brähler et al.[30] paticularly with a calcination phase performed at 1600°C for UO_2 crystallization. UO_2 TRISO particle constitutes a UO_2 based kernel (500 μm of diameter) composed by grains and grain boundaries (**Figure 1**). The grain

size has been measured between 10 and 20 µm. Other details about the characterization of the UO_2 TRISO particle sample can be found elsewhere[31].

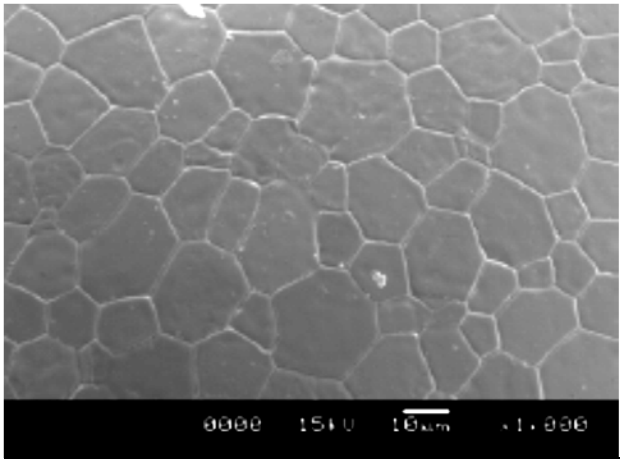

Figure 1: SEM picture of an unirradiated UO_2 particle surface.

In all the experiments, water used in this work is ultra pure water Millipore Alpha-Q with an electrical conductivity of 18.2 MΩ.

2.2. Experimental Conditions

$^4He^{2+}$ irradiation was performed at the ARRONAX cyclotron facility (Saint-Herblain, France). The $^4He^{2+}$ beam diameter was around 10 mm. The energy range was 64.5 or 66.5 MeV depending on the irradiation conditions with an average LET of 22.7 keV/µm. The energy of the $^4He^{2+}$ particles inside the irradiation cell is systematically evaluated by using the SRIM 2008 simulation code [32, 33]. In these calculations, all the obstacles upstream of the cell are taken into account. The intensity of the particles beam, measured on an internal Faraday cup located one meter upstream, was maintained at 70 nA. The uncertainty of the current measurement is about 10 %.

Irradiation was realized in two atmospheric conditions : I) open to air, II) closed with air and III) closed with Ar/H_2 atmospheres. The last one is considered as a reference and the main difference between these conditions is that in closed atmosphere, H_2 produced by water radiolysis is not evacuated. It can then interact with the UO_2 solid surface which is not

possible in open atmosphere due to gas evacuation during irradiation. The irradiation time was 1, 3, 5, 10, 15 and 20 min according to the desired dose.

2.2.1. Experimental Setup

The experimental setup consists of two compartments named Cell 1 and Cell 2. Cell 1 served as a container of the UO_2 particles which permitted their irradiation. It is made of Polypropylene (PP) with a removable cover of aluminium perforated in the middle to allow sample irradiation. After introducing the UO_2 particles in the Cell 1, the distance between the solid surface and the entrance window of the aluminium cover was 5 mm. It was chosen carefully to avoid direct irradiation of the UO_2 particles from one hand and to prevent its interaction with the radical species produced by water radiolysis from the other hand. Indeed this work is devoted to study the effect of the molecular species produced by water radiolysis onto the solid corrosion and not the consequences of direct irradiation of the solid or the effect of the radical species. As mentioned above, the $^4He^{2+}$ ions beam was provided by the ARRONAX cyclotron facility with E = 64.5 or 66.5 eV. For these two energies the average length of the $^4He^{2+}$ particles, calculated by the SRIM 2008 simulation code [32, 33], is not expected to exceed 3.5 mm in ultra-pure water used in this investigation. Thus, after filling the experimental setup by ultra-pure water, the direct effects of the $^4He^{2+}$ ions irradiation in the cell 1 occur onto the solution and not onto the solid surface (distance between UO_2 particles and $^4He^{2+}$ beam is 5 mm as described before). In case of irradiation in closed atmosphere, a borosilicate glass disc with a diameter of 25 mm and a thickness of 150 μm was placed between the cover and the PP Cell.

Cell 2 is a glass bottle with two necks: the first one contains a UV-VIS probe for *in-situ* dose rate determination and the second one is used for atmospheric conditioning of the experimental setup in close atmosphere experiments. In these latter conditions, the second neck of the Cell 2 was closed by a valve after atmospheric conditioning. The second neck can

also be connected to a GC (Gas Chromatography) device for gas analysis. The lower part of the Cell 2 has two outlets for connexion with the cell 1.

The two compartments of the experimental setup were connected by Viton hoses. A peristaltic pump was used for evacuation in closed atmosphere and to circulate the solution in order to ensure its homogenization in the whole system for all the atmospheres.

First of all, 200 particles of UO_2 were introduced in the Cell 1. Based on previous experimental tests, this number is sufficient to quantify any soluble uranium species which may be leached into the solution. 28 ml of ultra-pure water were then introduced in the Cell 2. This volume was chosen carefully to cover the optical path of the visible Ultra Violet (UV-VIS) probe and to ensure a sufficient void volume in the system for gas production (in closed atmosphere experiments).

For each experiment, the first step realized after irradiation was molecular hydrogen analysis (this step was absent for experiments realized in open-to-air atmosphere). Then, one UO_2 particle was retrieved and a volume of 3 ml of the irradiated solution was collected: 1 ml for H_2O_2 analysis, 1 ml for soluble uranium species analysis and 1 ml to stock the UO_2 particle in order to perform further kinetic solid analysis. 3 ml of ultra-pure water were later added to the system (before the next irradiation) to compensate the volume collected for solution analysis.

2.2.2. Dose Rate Determination

In this investigation, Super Fricke dosimetry[34] was used to determine the irradiation dose rate. This method is based on the oxidation of Fe^{2+} to Fe^{3+} by the species produced by water radiolysis. These measurements are carried out during irradiation (*in situ*). Super Fricke solutions are prepared by dissolving the desired quantity of ferrous sulphate (H_2SO_4, $[Fe^{2+}]$ = 10 mmol l^{-1}) and sodium chloride (NaCl) (1 mmol l^{-1}) in aerated aqueous 0.4 mol l^{-1} sulfuric acid (H_2SO_4) solutions. All reagents are analytical grade or equivalent. NaCl is added to

suppress any organic impurities. Fricke dose rate was found around 4370 Gy.min^{-1} using the ferric ion radiolytic yield from the literature[35]. In our conditions, the ferric ions yield G(Fe^{3+}) was 11.6 10^{-7} mol J^{-1}.

2.3. Measurment Techniques

2.3.1. UV-VIS Spectrophotometry

In this work, the Fricke dose rate and the concentrations of H_2O_2 produced by water radiolysis were determined by a CARY4000 (VARIAN) spectrophotometer. For the dose rate calculation, the concentration of ferric ions was monitored by UV-Vis measurements at 304 nm (ε = 2197 l mol^{-1} cm^{-1}). Concentrations of H_2O_2 have been determined after irradiation (about 15 min after the experiment), with the Ghormley triiodide method[36] using two reagents. One is a mixture of ammonium molybdate ($Mo_7O_{24}(NH_4)$ $2H_2O$, Carlo Erba), potassium iodide (KI, VWR) and sodium hydroxide (NaOH, VWR) and the second is a buffer solution (pH 4–5) of acid potassium phthalate ($C_8H_5KO_4$, VWR). For a total volume of 2 mL, 0.5 mL of both reagents was mixed with 1 mL of the sample solution. The concentration of H_2O_2 is obtained indirectly by measurement of I_3^- absorbance. The molar extinction coefficient of I_3^- at the 351 nm wavelength is previously determined at 25300 l mol^{-1} cm^{-1} in the studied solution at 298 K.

2.3.2. Inductively coupled Plasma Mass Spectrometry

After irradiation, the collected solutions were acidified adding 3 ml of pure nitric acid (HNO_3) 3 mol l^{-1} at 2% and analyzed by Inductively Coupled Plasma Mass Spectrometry (ICP-MS) to determinate the concentration of the soluble uranium species released into the solution. The detection limit of the apparatus is 10^{-9} mol l^{-1} with an uncertainty of 10% and the solvent is pure HNO_3 3 mol l^{-1} at 69%.

2.3.3. Micro Gas Chromatography

In the closed atmosphere experiments, molecular hydrogen produced by water radiolysis was measured by gas chromatography technique. The apparatus is a 490-GC, which is a l-GC model from VARIAN. The carrier gas was ultra-high purity argon (Ar) with a pressure of 150 kPa. The gas sample was introduced using a Swagelok connection and the injection volume is 10 µl. The column is a Molecular Sieve 5A (length = 4 m and diameter = 0.25 mm). The detection was performed using a thermal conductivity detector. Calibration of the detector is performed by injection of different gas mixture of Ar/H_2 with a proportion of H_2 varying from 0.1 to 5 mol l^{-1}. Uncertainty in gas measurements is estimated to be less than 10%.

2.3.4. Raman spectroscopy

Analysis of the solid UO_2 particles by Raman spectroscopy was performed after irradiation (around 20 min after the experiment). A kinetic solid analysis was then started by recording Raman spectra of the corroded particles as a function of time until the spectra remained stable (1 week). For each experiment, spectra were registered each hour at first and then each day.

All the Raman setup is purchased by the HORIBA Jobin–Yvon Company. Raman spectra are recorded with an iHR550 spectrometer equipped with two optical fibers (diameter = 100 µm, length = 20 m). The detector is a charged coupled device (CCD) cooled by Peltier effect (203 K). The samples are excited with a red laser beam at 632.8 nm emitted by a He/Ne Laser. The laser beam is focused on the samples by a near infra-red 100X Mitutoyo lens with a diameter of 24.6 mm and a power of 14 mW for a working distance of 12 mm from the sample and an acquisition time of 1 min. The spectral range studied was between 100 and 1400 cm^{-1}. The region beyond 900 cm^{-1} presents Raman bands characteristic of defects present in the UO_2 matrix[13, 37] and the spectrum of water which makes data analysis very difficult in this domain. Therefore this paper will present spectra in the interesting spectral range between 100 and 900 cm^{-1}. The Raman backscattering is collected through the same objective and dispersed by 1200 groves/mm gratings to reach 5 cm^{-1} spectral resolution for

Raman stokes spectra excited at 632.8 nm. The wavenumber accuracy has been checked and was better than 0.5 cm^{-1}.

2.3.5. Scanning Electron Microscopy

Before and after irradiation, the UO_2 particles were characterized by SEM (Scanning Electron Microscopy) in order to describe their surface and localize the corroded zones (grains or grain bourndaries). The SEM microscope used in this work is a JEOL 5800 SV with a voltage of 15 or 10 kV. The SEM samples were covered by a Pt layer in order to improve electron conduction and increase the picture resolution.

3. Data Treatment

3.1. Calculation of Raman Peak Area Ratios

Raman spectra were imported to Dmfit software 2010[38] in order to decomposed them in the spectral range between 100 and 900 cm^{-1}. Four Raman peaks were then obtained. For each peak "*i*", its area A_i is given by the software to overcome the relative peak intensity variation. Relative areas (named S_i) were calculated as follows:

$$S_i = \frac{A_i}{A_t} * 100 \quad (1)$$

where A_t is the total area of the Raman spectrum calculated according to equation (2) :

$$A_t = \sum_{i=1}^{i=4} A_i + A_{ap} \quad (2)$$

where A_{ap} is the Raman peak area of the adjustment peaks used to adjust the fit to the experimentally obtained Raman spectra.

3.2. Dissolution Rate

The dissolution rate r (g m^{-2} d^{-1}) of the oxidized phase can be defined as[39] :

$$r = \frac{V}{S}\frac{d[U]}{dt} M_{UO_2} \quad (3)$$

where V is the volume of the leaching solution (m^3), S is the total surface area of the solid (m^2), M_{UO2} is the molar mass of UO_2 and $d[U]/dt$ (mol m^{-3}) is the variation of soluble uranium species as a function of the irradiation time. V/S = 0.18 m, it was calculated by dividing the volume of the leaching solution on the surface of the 200 UO_2 particles. M_{UO2} = 270 g mol^{-1} and $d[U]/dt$ can be calculated from the slope of the curve representing the variation of soluble uranium species in the irradiated solution as a function of the irradiation time.

3.3. Chemical Radiolytic Yields

The radiolytic yield is defined as the number of species formed or disappeared per unit of deposited energy. It is expressed in the international system by μmol J^{-1} and is calculated at a time t after transition of the ionizing irradiation according to the equation (4) :

$$G_t(X) = \frac{X_t}{\rho D} \quad (4)$$

where $[X]_t$ is the concentration of the species X at the time t (mol l^{-1}), ρ is the density of the irradiated solution (kg l^{-1}) and D the absorbed dose (J kg^{-1}).

4. Results

4.1. UO_2 Surface Characterization

The spectrum of the unirradiated UO_2 is presented in **Figure 2**.

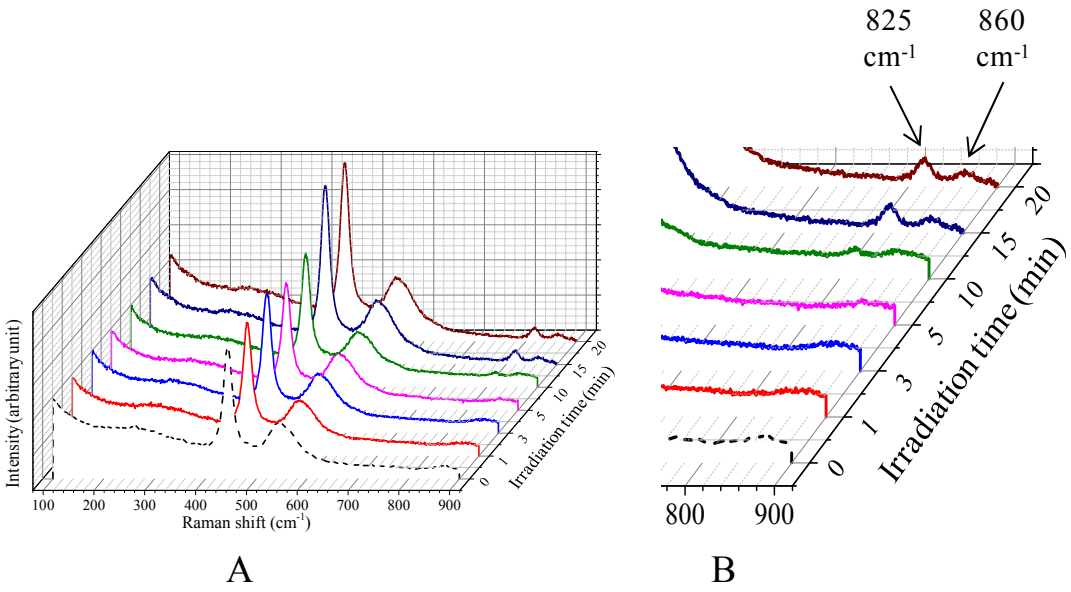

Figure 2: A) Raman spectra of a non-irradiated UO_2 particle (dotted line) and the particles corroded by water radiolysis in open atmosphere (Set I) as a function of the irradiation time. B) Zoom on the spectral region between 800 and 900 cm^{-1} where metastudtite is formed by oxidation of UO_2.

It presents two characteristic bands around 445 cm^{-1} and 560 cm^{-1}. The former is affected to the triply degenerated Raman active mode (T_{2g}) of U-O stretch [13, 40-41, 37] whereas the latter characterizes the defects present initially in the UO_2 fluorite structure[37].

To estimate the Raman spectral modifications brought by the radiolytic products of water in the different studied conditions, a comparison was performed between the UO_2 spectra before and after irradiation. The results showed that after irradiation in closed atmosphere (with air and with Ar/H_2), the spectra of the UO_2 particles remained stable as a function of the dose. That's why these spectra will not be presented in this paper. On the other hand, when water in contact with the UO_2 particles was irradiated in open to air atmosphere, no spectral modifications were observed until 21.8 kGy deposited in the solution (**Figure 2**). From 43.7 kGy, modifications can be seen between 800 and 900 cm^{-1} and appear clearly at the dose of 87.3 kGy. Indeed, two peeks appear at 825 and 860 cm^{-1}. Both of these bands characterize

the metastudtite ($UO_2(O_2)\ 2H_2O$) [13, 28, 29] formed on the UO_2 surface by oxidation with H_2O_2 produced by water radiolysis according to the reaction (**i**)[14] :

$$UO_2 + 2H_2O_2 \rightarrow UO_2(O_2)\ (H_2O)_2 \qquad \textbf{(i)}$$

After irradiation, kinetic analysis of the solid particles was realized by Raman spectroscopy as detailed previously. The results showed that Raman spectra of the samples irradiated with an irradiation time t = 1 min remained unchanged after two months of the experiment. It seems that in these conditions, UO_2 oxidation is very low due to low H_2O_2 concentration produced. The sensitivity of the Raman apparatus used does not permit to detect it. For $t \geq 3$ min, Raman spectra of the irradiated particles evolved slightly as a function of time until one week after irradiation and then remained stable. In this paper, we will discuss only the spectra that evolved as a function of time (until 1 week after irradiation). For instance, **Figure 3** displays the spectra recorded versus time after irradiation for the particles irradiated for 20 min under open to air atmosphere.

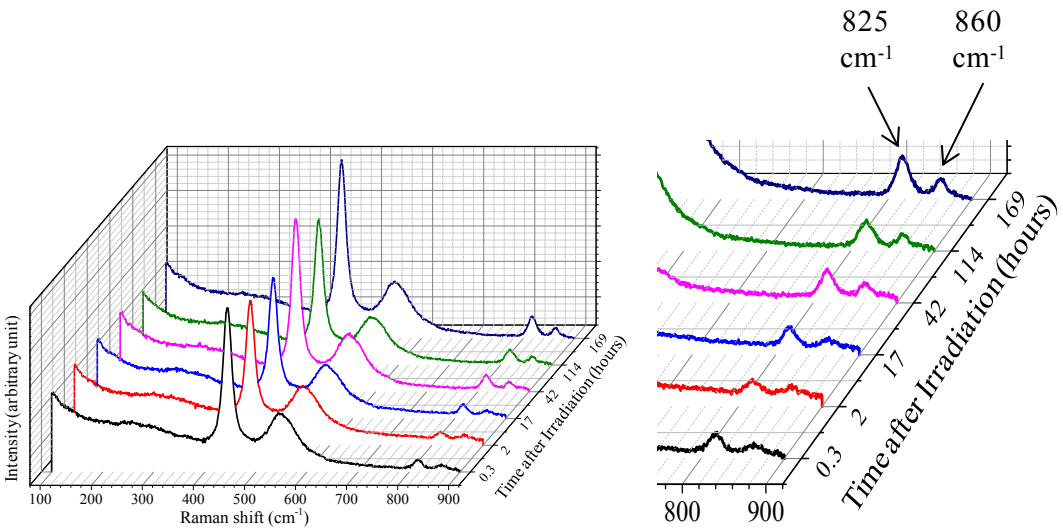

Figure 3: A) Evolution as a function of time after irradiation of the UO_2 Raman spectra for the samples irradiated during 20 min in open to air atmosphere (Set I). B) Zoom on the spectral region between 800 and 900 cm^{-1} where metastudtite is formed by oxidation of UO_2.

In order to analyze the temporal evolution of the UO_2 Raman spectra after irradiation, area ratios of the characteristic peaks observed at 445, 535, 820 and 865 cm^{-1} were calculated and are discussed below. A similar work was done by He and al.[42] who followed the variations of UO_2 Raman peak intensities as a function of matrix doping by fission products. Area ratios of the characteristic peaks at 445, 535, 820 and 865 cm^{-1}, designed here by S_1, S_2, S_3 and S_4 respectively, were calculated as a function of time as described before. Adjustment peaks area ratios were also calculated to verify that the sum of all the area ratios is equal to 100%. **Figure 4** shows the variation of the sum S_3+S_4 (area ratios of the peeks at 820 and 865 cm^{-1} characterizing the metastudtite) as a function of the irradiation time until one week after irradiation. Beyond one week, no significant variation of peek intensities was observed.

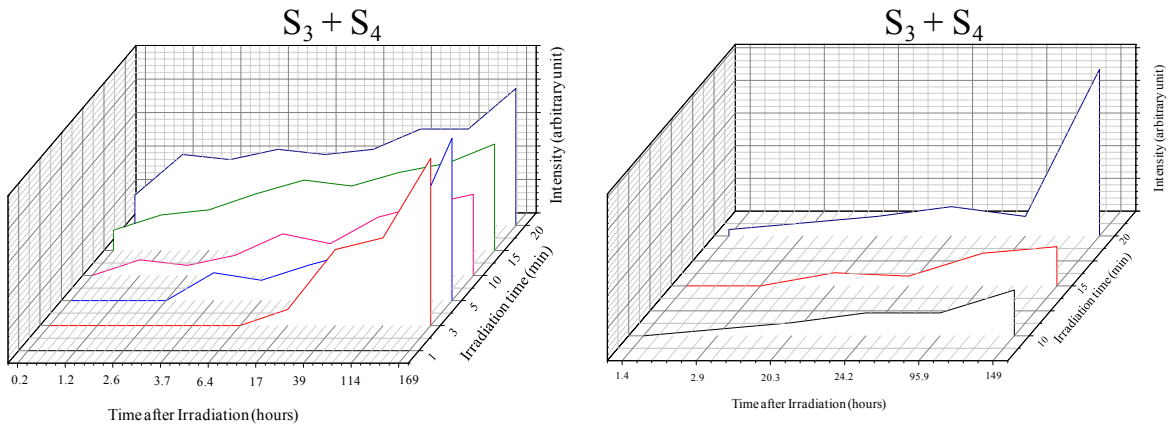

Figure 4: Evolution as a function of the irradiation time and until around one week after irradiation of the area ratios S_3+S_4 characterizing the metastudtite in open (A) and closed (B) atmosphere.

Regardless the irradiation atmosphere, S_3 + S_4 characterizing the metastudtite formed by oxidation of the UO_2 surface increased with both the irradiation time and the time after irradiation. However, this increasing is delayed after H_2 evacuation in closed atmosphere which confirms that this gas has an inhibition effect on the corrosion process.

4.2. Uranium Solubility and Dissolution Rate

After irradiation, water in contact with the UO_2 particles was collected to quantify the soluble uranium species leached into the solution. Indeed, the metastudtite phase formed on the surface of UO_2 after oxidation by H_2O_2 produced by water radiolysis underwent later a dissolution step where uranyl ions (UO_2^{2+}) were leached into the solution. The mechanism of this dissolution reaction in ultra-pure water was rarely discussed in the literature. According to some authors[23], the dissolution step occurs according to reaction (ii) :

$$UO_2^{2+}{}_{(s)} + H_2O \rightarrow UO_2(OH)^+ + H^+ \qquad \textbf{(ii)}$$

However, Sattonay et al.[23] proposed this dissolution mechanism based on a pH decreasing observed in their case after the solution irradiation. But, in our work, measurement of the irradiated solutions acidity after each irradiation showed that pH did not evolve and remained between 6.5 ± 0.5 and 7.5 ± 0.5. This means that the above proposed mechanism (reaction (ii)) does not occur in our case.

Figure 5 shows the variation of the soluble uranium species concentration leached into the solution after irradiation as a function of the dose and the irradiation time in both open and closed atmosphere.

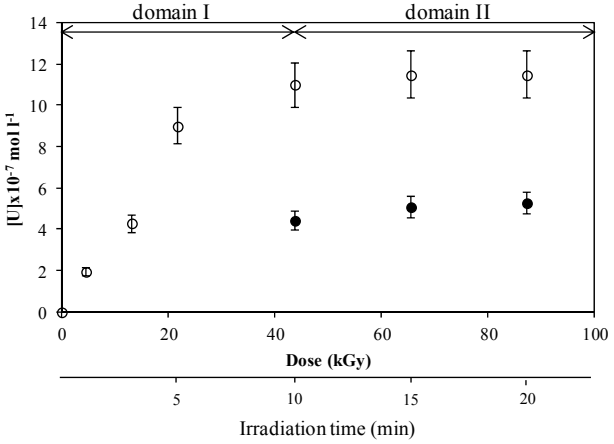

Figure 5: Variation of the concentration of soluble uranium leached to the irradiated solution versus the absorbed dose in open (○) and closed with air (●) atmosphere.

Regardless the irradiation atmosphere, the quantity of soluble uranium species increased with the dose and then remained constant from 43.6 kGy. At this latter dose, concentration of soluble uranium species found in closed atmosphere ($4.5 \pm 0.5\ 10^{-7}$ mol l^{-1}) is two-fold lower than that observed in open atmosphere ($11.0 \pm 1.0\ 10^{-7}$ mol l^{-1}) due to the inhibition of the UO_2 oxidation by H_2 produced by water radiolysis. **Figure 5** shows too the variation of the [U] with respect to the irradiation time for each set of samples. Two domains can be seen : the first one is for an irradiation time between 0 and 10 min (domain I) with a higher leaching rate, the second one is for an irradiation time beyond 10 min (domain II) with either lower leaching rate or approach to steady state concentration values. The final steady state of [U] values measured in our system are presented in **Table 1** for an irradiation time of 10 min together with the normalized leaching rate (r) obtained from the domain I. Moreover, Table 1 presents also UO_2 solubility values obtained from literature in order to compare it to our data.

Table 1: Steady state U concentrations, Dissolution rate and factor (r and r') of UO_2 and experimental conditions used in this study and others found in the literature.

Ref.	Physical aspect UO_2	$^4He^{2+}$ Beam	Dose Rate Gy min^{-1}	Atm.	[U] 10^{-7} mol l^{-1}	Diss. rate r mg m^{-2} d^{-1}	Diss. factor r' µg m^{-2} Gy^{-1}
This work	Particles	External source*	4370	Ox	11.49	13500	2.01
				Red	5.25	7000	1.11
[6]	Pellet	Internal		Ox		0.5	
[39]	Particles	No	0	Red		23.3	
[24]	Colloids	External source*	52.7	Red		15.7	0.246
[43]	Pellets	Internal**	18	Ox		2.5	0.095
			1.8	Ox		0.2	0.076

* $^4He^{2+}$ Beam produced by cyclotron facility

** Doped UO_2 with Pu

When UO_2 particles were irradiated between 10 and 20 min in closed atmosphere, concentration of uranium species remained practically constant (**Figure 5**). Indeed the obtained values were respectively 4.5 ± 0.5 10^{-7} and 5.2 ± 0.5 10^{-7} mol l^{-1} for the latter mentioned irradiation time. These values are comparable to most solubility data reported in the literature[6, 24, 39, 43]. However, we believe that in our work the thermodynamic equilibrium of the UO_2 dissolution was not achieved due to their composition of grains and grain boundaries. We could calculate, in these conditions, the dissolution rate which was equal to 13.5 g m^{-2} d^{-1}. A comparison of our dissolution rates (domain I on **Figure 5**) with the literature data is given in **Table 1**. Despite the similarity with [U] reported in the literature, r values obtained in this investigation are at least 10^3 fold higher. It seems then that with the irradiation conditions used in our work, the UO_2 oxidation/dissolution mechanism occurred with a faster kinetic. This is very probably due to the impact of the high doses deposited in this work into the irradiated solution. In order to apprehend the dose impact on the UO_2 corrosion, we propose here a new methodology to express the dissolution rate. This methodology consists in calculating the dissolution rate as a function of the dose deposited into the solution and not as a function of the irradiation time. Thus, the new dissolution factor r' can be defined as follow :

$$r' = \frac{V}{S}\frac{d[U]}{dd}M_{UO_2} \qquad \textbf{(5)}$$

where *d[U]/dd* (mol m^{-3}) is the variation of soluble uranium species as a function of the dose deposited into the solution. In our case the r' values are 2.0 µg m^{-2} Gy^{-1} for the open atmosphere experiments and 1.1 µg m^{-2} Gy^{-1} for the closed atmosphere ones. These results confirm that the reducing atmosphere (in presence of H_2) has a strong diminishing impact onto the UO_2 dissolution rate. Moreover, **Table 1** displays the dissolution factor r' obtained by previous data[24, 43] in order to compare it to our results. Even after taking into account the effect of the absorbed dose, the values obtained in this work still higher than those reported in

the literature (**Table 1**). However, in our investigation, we used a very high dose rate (4370 $Gy.min^{-1}$) which certainly influences the UO_2 dissolution. It appears clearly then that the dose rate is the main parameter which controls the UO_2 dissolution rate.

4.3. H_2 and H_2O_2 Chemical Yields

When the ultra-pure water above the UO_2 particles was irradiated in closed air atmosphere, H_2 produced by water radiolysis was quantified by calculating its radiolytic yield (G) in order to compare it to that of pure water and explain any gas consumption by the inhibition of the UO_2 corrosion process. As described previously, the solution used during irradiation is ultra-pure water (ρ = 1 kg l^{-1}) and the mean $G(H_2)$ was 0.02 ± 0.002 µmol J^{-1}. It corresponds to the slope of the curve in **Figure 6** representing the variation of $[H_2]$ measured by µ-GC as a function of the dose.

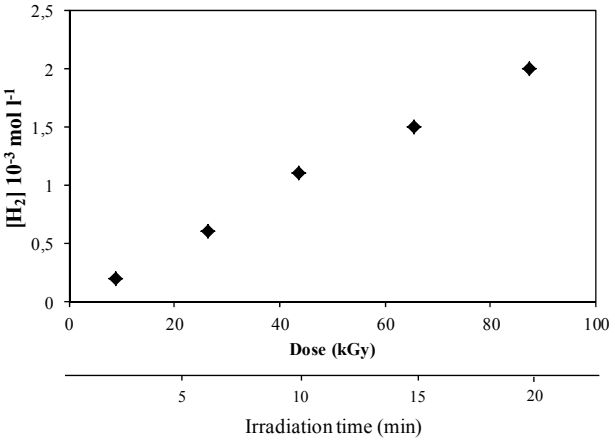

Figure 6: Variation of the concentration of H_2 produced by water radiolysis in closed with air atmosphere versus the dose.

Crumière et al.[44] irradiated ultra-pure water by a cyclotron $^4He^{2+}$ beam with an energy of 64.7 MeV and doses up to 800 Gy in Argon saturated atmosphere. $G(H_2)$ obtained in their work was 0.061 ± 0.006 µmol J^{-1} which is three-fold higher than that found in this investigation ($G(H_2)$ = 0.02 ± 0.002 µmol J^{-1}). The irradiation conditions used by Crumière et al.[44] are very similar to those used in our work which means that for the system UO_2/ultra-

pure water, a non negligible part (around 2/3) of the H_2 produced by water radiolysis was consumed certainly by inhibition of the UO_2 oxidation process.

In both open and closed to air atmospheres, concentrations of H_2O_2 produced by water radiolysis was determined by the Ghormley method[36], as described into the experimental section, to analyze the effect of the irradiation atmosphere on its consumption by the UO_2 oxidation. **Figure 7** presents the variation of $[H_2O_2]$ produced by water radiolysis under open and closed atmospheres as a function of the dose.

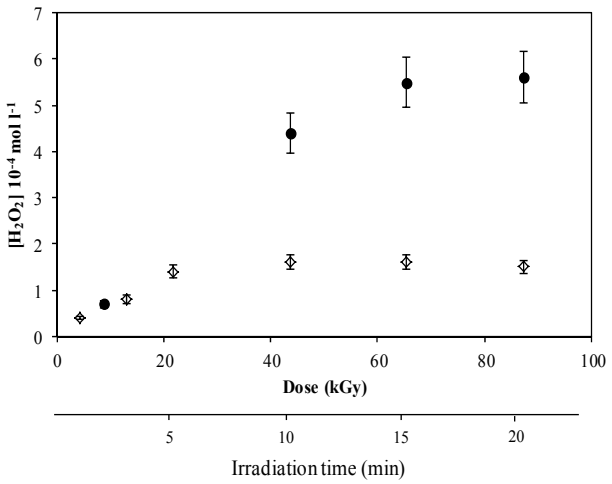

Figure 7: Variation of the concentration of H_2O_2 produced by water radiolysis versus the absorbed dose in open (○) and closed to air (●) atmosphere.

It shows that in both open and closed atmospheres, $[H_2O_2]$ produced by water radiolysis increased with the dose and then reached a steady state from 21.8 kGy and 65.5 kGy in open and closed atmosphere respectively. At these latter doses, the value of $[H_2O_2]$ were respectively $1.4 \pm 0.2\ 10^{-4}$ and $5.6 \pm 0.6\ 10^{-4}$ mol l^{-1} which means that the quantity of H_2O_2 was four-fold higher when the UO_2 particles were irradiated in closed atmosphere. It seems then that in the latter conditions consumption of H_2O_2 and thus oxidation of the UO_2 surface was inhibited by H_2 produced by water radiolysis. Radiolytic yields of H_2O_2 were also calculated and the values obtained were 0.06 ± 0.006 and 0.1 ± 0.01 µmol J^{-1} in open and closed atmosphere respectively (**Figure 7**). It appears then that in presence of H_2, $G(H_2O_2)$

was equal to that found for ultra-pure water [45-46] (0.102 μmol J^{-1}) irradiated by $^{4}He^{2+}$ beam. This confirms that in closed atmosphere, H_2O_2 was not consumed and oxidation of UO_2 was limited.

5. Discussion

From a macroscopic point of view, corrosion of UO_2 by the radiolysis products of water, in particularly by H_2O_2, occurs according to a two-step process. It starts by oxidation of the UO_2 surface leading to the formation of an oxidized metastudtite phase on the material surface (reaction i). The oxidized phase undergoes later a dissolution step (reaction ii) resulting in migration of uranyl ions into the solution.

Raman spectroscopic analysis realized after irradiation on the UO_2 particles confirmed that the oxidized phase formed on the surface was metastudtite ($UO_2(O_2)$ $2H_2O$)) which is consistent with the data reported in the literature[28]. In recent works[28, 29] on oxidation of UO_2 exposed to water radiolysis, the authors detected by *in situ* Raman spectroscopy the formation of schoepite beside metastudtite which was not observed in our case. However, in their investigation, the whole system (water + UO_2 matrix) was irradiated whereas in our work only water in contact with the UO_2 particles was irradiated. The spectroscopic analysis performed in our work also showed that when water in contact with the UO_2 particles was irradiated in closed atmospheres, the oxidation step during irradiation was limited due to its inhibition by H_2 produced by water radiolysis. Few days after irradiation in these latter conditions, in particular after H_2 evacuation, oxidation of the UO_2 surface and formation of metastudtite took place again which confirms that this gas has an inhibition effect on the corrosion process. This result is consistent with the analytical characterization of the irradiated solution which showed two-fold lower uranium releasing, four-fold higher quantity of H_2O_2 and consumption of H_2 produced by water radiolysis in closed atmosphere. In this

latter condition, the higher quantity of H_2O_2 and the consumption of H_2 observed let us conclude that the inhibition process did not occur by direct action of H_2 on the oxidant but by interaction between the H_2 produced by water radiolysis and the UO_2 surface. This result can be confirmed by the work of Pastina and Laverne[47] who studied the effect of H_2 on H_2O_2 production in $^4He^{2+}$ radiolysis of water. They showed that 800 µM of H_2 has no effect on the production of H_2O_2 which reinforce our hypothesis supposing that H_2 did not react directly with H_2O_2. Besides, some authors[48] reported that the UO_2 surface itself can act as a catalyst of dissolved hydrogen causing the reduction of any oxidized phase (U(VI)) formed by oxidation with H_2O_2 to its reduced form (U(IV)). This catalytic process cannot be excluded in our case; however, concentration of H_2O_2 observed in closed atmosphere was four-fold higher than that found in open atmosphere which means that the latter process, if held, was not the principal inhibition path. Another explanation of the absence of oxidation in closed atmosphere may be considered when taking into account possible interactions between the UO_2 surface and dissolved H_2 molecules (e.g. hydrogen bonds) which may form a sort of barrier preventing H_2O_2 from arriving to the UO_2 surface and oxidize it as presented on **Figure 8**.

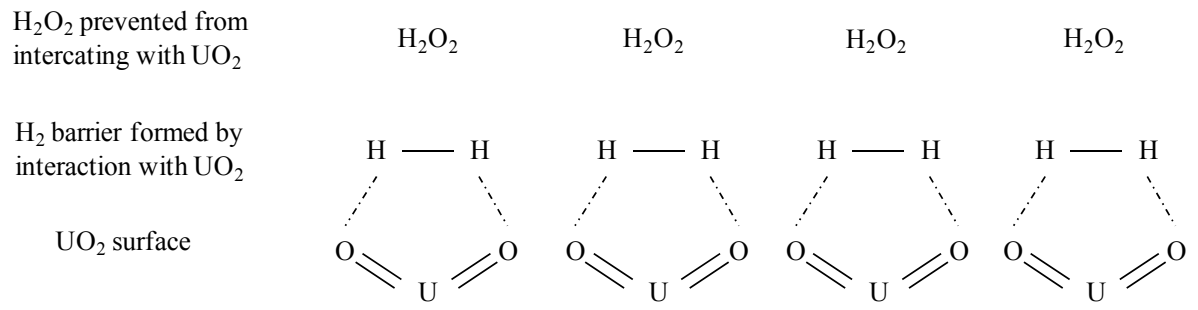

Figure 8: Representation of possible interactions (hydrogen bonds) between dissolved H_2 and the UO_2 surface preventing the oxidation of this latter by H_2O_2 produced by water radiolysis.

These interactions may increase the solubility of H_2 in water which may explain the low $G(H_2)$ value obtained in our work after irradiation in closed atmosphere comparing to $G(H_2)$ for pure water (around 1/3). This hypothesis may be reinforced by the fact that the solubility

of H_2 in water (1.535 10^{-3} mol l^{-1} at 25°C and 1 bar) is of the order of magnitude of H_2 concentrations produced by water radiolysis in this work.

The data reported in the literature about soluble uranium species leached into the solution by radiolytic corrosion of UO_2 is rare and comparison to our results is very difficult due to the differences in the irradiation conditions. In a recent work, Trummer et al.[27] studied by simulation the effect of H_2 on the radiation induced dissolution of UO_2-base spent fuel. The concentration of soluble uranium species in the solution was around 10^{-10} mol l^{-1} for a dose between 3.2 and 17.1 kGy and a H_2 pressure of 40 bar. This value is lower than that obtained in our work (around 5.2 10^{-7} mol l^{-1}) when the UO_2 particles were corroded in closed atmosphere with a dose between 43.7 and 87.3 kGy. However, we should note that the difference in the values may be due to the differences in the experimental conditions between the two works, in particular the dose rate effect which is the main parameter controlling the radiolytic corrosion of UO_2.

Concerning UO_2 dissolution rates, it appears from **Table 1** that the dissolution rate of UO_2 depends largely on the irradiation conditions, in particular, the dose rate and the irradiation atmosphere. However, we can consider that the steady state of the uranium concentration obtained in this work is comparable to those reported in the literature despite the differences in the irradiation conditions.

Besides, SEM pictures were realized on the surface particles after irradiation in order to determine the zones most affected by the corrosion process. Regardless the irradiation atmosphere, the grain boundaries are a lot more degraded than the UO_2 grains. For instance, **Figure 9** shows the surface of a UO_2 particle irradiated in open atmosphere at a dose of 87.3 kGy.

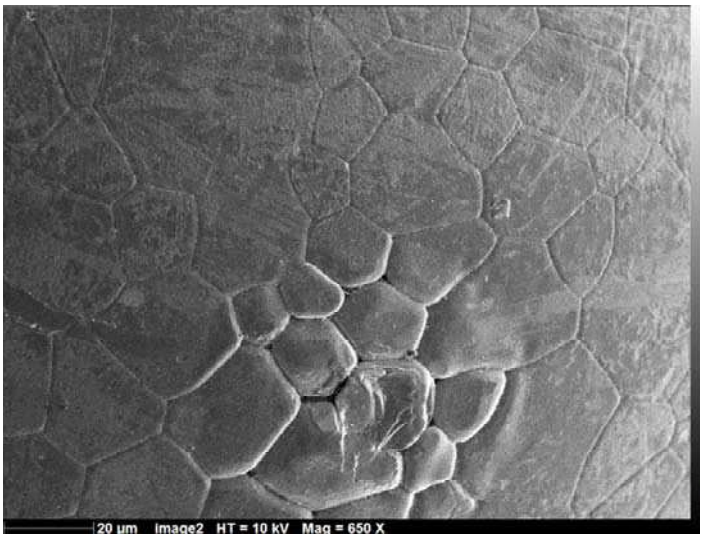

Figure 9: SEM picture of the surface of UO_2 particles corroded in open atmosphere.

The corrosion did not occur then homogeneously on the entire surface. Some regions of the grains surface are indeed more corroded.

Finally, as mentioned before, it is not actually possible to have a detailed mechanism of the oxidative dissolution of UO_2 particles by the radiolysis products of water. Thus, determining the kinetic constant of the different steps of this mechanism is not neither possible. On the other hand, in order to have a complete understanding of the radiolytic corrosion of UO_2, further studies will be later performed with pulse $^4He^{2+}$ beam to determine the effect of the radical species produced by water radiolysis on UO_2 corrosion. Indeed, this type of experiment will permit us to measure the radical species produced during irradiation (e.g. $OH^{\bullet}$) and determine their role in the radiolytic corrosion of UO_2.

6. Conclusion

This work was done to study the effect of the molecular species produced by $^4He^{2+}$ beam radiolysis of water on UO_2 corrosion. For that, UO_2 particles were covered by ultra-pure water and the $^4He^{2+}$ beam was monitored so that only the liquid was irradiated.

After irradiation, the effect of the molecular species was investigated by characterizing the corroded solid particles, quantifying H_2 and H_2O_2 produced by water radiolysis and measuring the soluble uranium species migrated to the solution. The influence of two parameters was investigated: the absorbed dose and the oxidant/reducing character of the irradiation atmosphere. In open atmosphere, corrosion of UO_2 started with an oxidation step byH_2O_2 produced by water radiolysis, which leaded to the formation of a metastudtite phase on the particles surface. The oxidized phase underwent later a dissolution reaction which resulted in migration of soluble uranium into the solution. In closed atmospheres, UO_2 corrosion was limited due to the inhibition effect of H_2: metastudtite was not observed, $[H_2O_2]$ was four fold higher, [U] was twofold lower and 2/3 of H_2 produced by water radiolysis was consumed. H_2 did not react then with H_2O_2 but directly interacted with the UO_2 surface. The inhibition process may occur by adsorption of H_2 on the material surface which prevents H_2O_2 from oxidizing it.

Dissolution rate of the soluble uranium leached into the irradiated solution were also calculated in this work as a function of the time and the absorbed dose. The dissolution rate values were lower in presence of H_2. These values depend on the irradiation conditions, in particular the dose rate which is the main parameter influencing it.

After irradiation, SEM pictures realized on the UO_2 particles showed that the corrosion did not take place homogeneously on the particles surface. The grain boundaries were more corroded than the grains.

Further studies will be later performed with pulse $^4He^{2+}$ beam to determine the effect of the radical species produced by water radiolysis on UO_2 corrosion. This will permit us to have a global radiolytic data and a complete understanding of UO_2 corrosion.

AUTHOR INFORMATION

Corresponding Author

*To whom correspondence should be addressed. Phone: (+33) 2 51 85 85 36. Fax: (+33) 2 51 85 84 52. E-mail: johan.vandenborre@subatech.in2p3.fr.

ACKNOWLEDGMENT

We thank N. Stephant and J.Y. Mevellec from the IMN laboratory for their support in the Raman measurements and for letting us perform SEM analysis. The authors acknowledge financial support from the French National Research Agency (ANR) in the project CISSRAD ALPHA (ANR-JCJC-2011 CISSRAD ALPHA) for their financial support. This research has also received funding from the European Union's European Atomic Energy Community's (Euratom) Seventh Framework Programme FP7/2007-2011 under grant agreement n° 295722 (FIRST-Nuclides project). We also thank the ARRONAX staff for the efficient performing of irradiation runs onto the cyclotron facilities.

REFERENCES

1. Carbol, P.; Fors, P.; Van Winckel, S.; Spahiu, K., Corrosion of Irradiated MOX Fuel in presence of Dissolved H_2. *J. Nucl. Mat.* **2009,** *392*, 45-54.

2. Sunder, S.; Shoesmith, D. W.; Christensen, H.; Miller, N. H., Oxidation of UO_2 Fuel by the Products of γ Radiolysis of Water. *J. Nucl. Mat.* **1992,** *190*, 78-86.

3. Röllin, S.; Spahiu, K.; Eklund, U. B., Determination of Dissolution Rates of Spent Fuel in Carbonate Solutions under different Redox Conditions with a Flow-through Experiment. *J. Nucl. Mat.* **2001,** *297*, 231-243.

4. Amme, M., Contrary Effects of the Water Radiolysis Product H_2O_2 upon the Dissolution of Nuclear Fuel in Natural Ground Water and Deionized Water. *Radiochim. Acta* **2002,** *90*, 399-406.

5. Biwer, B. M.; Ebert, W. L.; Bates, J. K., The Raman Spectra of several Uranyl-containing Minerals using a Microprobe. *J. Nucl. Mat.* **1990,** *175*, 188-193.

6. Shoesmith, D. W.; Sunder, S., The Prediction of Nuclear Fuel (UO_2) Dissolution Rates under Waste Disposal Conditions. *J. Nucl. Mat.* **1992,** *190*, 20-35.

7. Allen, A. O., *The Radiation Chemistry of Water and Aqueous Solutions*. Princeton, USA, 1961.

8. Spotheim-Maurizot, M.; Mostafavi, M.; Douki, T.; Belloni, J., *Radiation Chemistry : From Basics to Applications in Material and Life Sciences*. EDP Sciences: Les Ulis, France, 2008.

9. Christensen, H.; Sunder, S., Current State of Knowledge of Water Radiolysis Effects on Spent Nuclear Fuel Corrosion. *Nucl. Technol.* **2000,** *131*, 102-123.

10. Shoesmith, D. W., Fuel Corrosion Processes under Waste Disposal Conditions. *J. Nucl. Mat.* **2000,** *282*, 1-31.

11. Broczkowski, M. E.; Noël, J. J.; Shoesmith, D. W., The Inhibiting Effects of Hydrogen on the Corrosion of Uranium Dioxide under Nuclear Waste Disposal Conditions. *J. Nucl. Mat.* **2005,** *346*, 16-23.

12. Wren, J. C.; Shoesmith, D. W.; Sunder, S., Corrosion Behavior of Uranium Dioxide in Alpha Radiolytically Decomposed Water. *J. Electrochem. Soc.* **2005,** *152*, B470-B481.

13. Amme, M.; Renker, B.; Schmid, B.; Feth, M. P.; Bertagnolli, H.; Döbelin, W., Raman Microspectrometric Identification of Corrosion Products formed on UO_2 Nuclear Fuel during Leaching Experiments. *J. Nucl. Mat.* **2002,** *306*, 202-212.

14. Corbel, C.; Sattonnay, G.; Guilbert, S.; Garrido, F.; Barthe, M. F.; Jegou, C., Addition versus Radiolytic Production Effects of Hydrogen Peroxide on Aqueous Corrosion of UO_2. *J. Nucl. Mat.* **2006,** *348*, 1-17.

15. Jégou, C.; Muzeau, B.; Broudic, V.; Poulesquen, A.; Roudil, D.; Jorion, F.; Corbel, C., Effect of Alpha Irradiation on UO_2 Surface Reactivity in Aqueous Media. *Radiochim. Acta* **2005,** *93*, 35-42.

16. Suzuki, T.; Abdelouas, A.; Grambow, B.; Mennecart, T.; Blondiaux, G., Oxidation and Dissolution Rates of UO_2(s) in Carbonate-rich Solutions under External α Irradiation and Initially Reducing Conditions. *Radiochim. Acta* **2006,** *94*, 567-573.

17. Carbol, P.; Fors, P.; Gouder, T.; Spahiu, K., Hydrogen Suppresses UO_2 Corrosion. *Geochim. Cosmochim. Acta* **2009,** *73*, 4366-4375.

18. Ekeroth, E.; Roth, O.; Jonsson, M., The Relative Impact of Radiolysis Products in Radiation Induced Oxidative Dissolution of UO_2. *J. Nucl. Mat.* **2006,** *355*, 38-46.

19. Roth, O.; Jonsson, M., Oxidation of UO_2 (s) in Aqueous Solution. *Centr. Europ. J. Chem.* **2008,** *6*, 1-14.

20. Carbol, P.; Cobos-Sabate, J.; Glatz, J. P.; Ronchi, C.; Rondinella, V.; Wegen, D. H.; Wiss, T.; Loida, A.; Metz, V.; Kienzler, B., et al. *The Effect of Dissolved Hydrogen on the*

Dissolution of ^{233}U doped UO_2(s), High Burn-up Spent Fuel and MOX Fuel; TR-05-09; SFS EU-Project: Stockholm, 2005.

21. Christensen, H.; Sunder, S.; Shoesmith, D. W., Oxidation of Nuclear Fuel (UO_2) by the Products of Water Radiolysis: Development of a Kinetic Model. *J. Alloys Compd.* **1994,** *213-214*, 93-99.

22. Sunder, S.; Boyer, G. D.; Miller, N. H., XPS Studies of UO_2 Oxidation by α Radiolysis of Water at 100°C. *J. Nucl. Mat.* **1990,** *175*, 163-169.

23. Sattonnay, G.; Ardois, C.; Corbel, C.; Lucchini, J. F.; Barthe, M. F.; Garrido, F.; Gosset, D., α-Radiolysis Effects on UO_2 Alteration in Water. *J. Nucl. Mat.* **2001,** *288*, 11-19.

24. Grambow, B.; Mennecart, T.; Fattahi, M.; Blondiaux, G., Electrochemical Aspects of Radiolytically Enhanced UO_2 Dissolution. *Radiochim. Acta* **2004,** *92*, 603-609.

25. Mennecart, T.; Grambow, B.; Fattahi, M.; Andriambololona, Z., Effect of α Radiolysis on doped UO_2 Dissolution under Reducing Conditions. *Radiochim. Acta* **2004,** *92*, 611-615.

26. Sunder, S.; Shoesmith, D. W.; Miller, N. H., Oxidation and Dissolution of Nuclear Fuel (UO_2) by the Products of the α Radiolysis of Water. *J. Nucl. Mat.* **1997,** *244*, 66-74.

27. Trummer, M.; Jonsson, M., Resolving the H_2 Effect on Radiation Induced Dissolution of UO_2-based Spent Nuclear Fuel. *J. Nucl. Mat.* **2010,** *396*, 163-169.

28. Guimbretière, G.; Canizares, A.; Simon, P.; Tobon-Correa, Y. A.; Ammar, M. R.; Corbel, C.; Barthe, M. F., In-Situ Raman Observation of the First Step of Uranium Dioxide Weathering Exposed to Water Radiolysis. *Spectrosc. Lett.* **2011,** *44*, 570-573.

29. Canizarès, A.; Guimbretière, G.; Tobon, Y. A.; Raimboux, N.; Omnée, R.; Perdicakis, M.; Muzeau, B.; Leoni, E.; Alam, M. S.; Mendes, E., et al., In situ Raman Monitoring of Materials under Irradiation: Study of Uranium Dioxide Alteration by Water Radiolysis. *J. Raman Spectrosc.* **2012,** *43*, 1492-1497.

30. Brähler, G.; Hartung, M.; Fachinger, J.; Grosse, K.-H.; Seemann, R., Improvements in the Fabrication of HTR Fuel Elements. *Nucl. Eng. Des.* **2012**.

31. Kienzler, B.; Metz, V.; Duro, L.; Valls, A., Collaborative Project "Fast / Instant Release of Safety Relevant Radionuclides from Spent Nuclear Fuel" , Budapest 09 - 11 October 2012 (KIT Scientific Reports ; 7639). *Proceedings 1st Annual Workshop (7th EC FP CP FIRST-Nuclides)* **2012**.

32. Ziegler, J. F.; Biersack, J. P.; Littmark, U., *The Stopping and Range of Ions in Matter*. Pergamon Press: New York, USA, 1985.

33. Ziegler, J. F.; Ziegler, M. D.; Biersack, J. P., SRIM The Stopping and Range of Ions in Matter *Nucl. Instrum. Methods Phys. Res., Sect. B* **2010,** *268*, 1818-1823.

34. Fricke, H.; Hart, E. J., *Chemical Dosimetry, Radiation Dosimetry*. Academic Press: New York, USA, 1966.

35. Costa, C.; Vandenborre, J.; Crumière, F.; Blain, G.; Essehli, R.; Fattahi, M., Chemical Dosimetry during Alpha Irradiation: A Specific System for UV-Vis in situ Measurement *Am. J. Anal.Chem.* **2012,** *3*, 6-11.

36. Ghormley, J. A.; Hochanadel, C. J., The Yields of Hydrogen and Hydrogen Peroxide in the Irradiation of Oxygen saturated Water with Cobalt γ-Rays. *J. Am. Chem. Soc.* **1954,** *76*, 3351-3352.

37. He, H.; Shoesmith, D., Raman Spectroscopic Studies of Defect Structures and Phase transition in Hyper-stoichiometric UO_{2+x}. *Phys. Chem. Chem. Phys.* **2010,** *12*, 8108-8117.

38. Massiot, D.; Fayon, F.; Capron, M.; King, I.; Le Calvé, S.; Alonso, B.; Durand, J.-O.; Bujoli, B.; Gan, Z.; Hoatson, G., Modelling One- and Two-dimensional Solid-state NMR Spectra. *Magn. Reson. Chem.* **2002,** *40*, 70-76.

39. Casas, I.; de Pablo, J.; Clarens, F.; Giménez, J.; Merino, J.; Bruno, J.; Martinez-Esparza, A., Combined Effect of H_2O_2 and HCO_3^- on UO_2(s) Dissolution Rates under Anoxic Conditions. *Radiochim. Acta* **2009,** *97*, 485-490.

40. Amme, M.; Wiss, T.; Thiele, H.; Boulet, P.; Lang, H., Uranium Secondary Phase formation during Anoxic Hydrothermal Leaching Processes of UO_2 Nuclear Fuel. *J. Nucl. Mat.* **2005,** *341*, 209-223.

41. Manara, D.; Renker, B., Raman Spectra of Stoichiometric and Hyperstoichiometric Uranium Dioxide. *J. Nucl. Mat.* **2003,** *321*, 233-237.

42. He, H.; Keech, P. G.; Broczkowski, M. E.; Noel, J. J.; Shoesmith, D. W., Characterization of the Influence of Fission Product doping on the Anodic Reactivity of Uranium Dioxide. *Can. J. Chem.* **2007,** *85*, 702-713.

43. Jégou, C.; Broudic, V.; Poulesquen, A.; Bart, J. M., Effects of α and γ Radiolysis of Water on Alteration of the Spent UO_2 Nuclear Fuel Matrix. *MRS Online Proceedings Library* **2003,** *807*.

44. Crumière, F.; Vandenborre, J.; Essehli, R.; Blain, G.; Barbet, J.; Fattahi, M., LET Effects on the Hydrogen Production induced by the Radiolysis of pure Water. *Radiat. Phys. Chem.* **2013,** *82*, 74-79.

45. LaVerne, J. A., *Radiation Chemical Effects of Heavy Ions, in Charged Particle and Photon Interactions - Chemical, Physicochemical, and Biological consequences with applications*. New York, USA, 2004.

46. Yamashita, S.; Katsumura, Y.; Lin, M.; Muroya, Y.; Miyazaki, T.; Murakami, T., Water Radiolysis with Heavy Ions of Energies up to 28 GeV.: 1. Measurements of Primary g Values as Track Segment Yields. *Radiat. Phys. Chem.* **2008,** *77*, 439-446.

47. Pastina, B.; LaVerne, J. A., Effect of Molecular Hydrogen on Hydrogen Peroxide in Water Radiolysis. *J. Phys. Chem. A* **2001,** *105*, 9316-9322.

48. Spahiu, K.; Werme, L.; Eklund, U. B., The Influence of near Field Hydrogen on Actinide Solubilities and Spent Fuel Leaching. *Radiochim. Acta* **2000,** *88*, 507.

Synopsis Toc

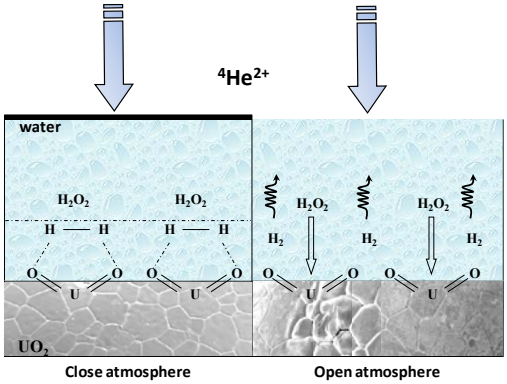

Authors have experimentally and quantitatively evidenced that the radiolytic corrosion of UO_2 is inhibited by the H_2 produced by the water radiolysis.